


Chemotherapeutic Effect of SR9009, a REV-ERB Agonist, on the Human Glioblastoma T98G Cells

ASN Neuro
Volume 11: 1–14
© The Author(s) 2019
Article reuse guidelines:
sagepub.com/journals-permissions
DOI: 10.1177/1759091419892713
journals.sagepub.com/home/asn


Paula M. Wagner^{1,2}, Natalia M. Monjes^{1,2}, and Mario E. Guido^{1,2} 

Abstract

Glioblastoma multiforme is the most aggressive brain tumor, and human T98G cells constitute a useful glioblastoma multiforme model to evaluate the chemotherapeutic agents. Modern life (shiftwork, jetlag, etc.) may cause circadian disorganization promoting higher cancer risk and metabolic disorders. Although little is known about the tumor-intrinsic circadian clock function, pharmacological modulation of circadian components may offer selective anticancer strategies. REV-ERBs are heme-binding circadian clock components acting as repressors of processes involved in tumorigenesis such as metabolism, proliferation, and inflammation. A synthetic pyrrole derivative (SR9009) that acts as REV-ERBs-specific agonists exhibits potent *in vivo* activity on metabolism and tumor cell viability. Here, we investigated SR9009 effects on T98G cell viability, differential chemotherapy time responses, and underlying metabolic processes (reactive oxygen species [ROS] and lipid droplets [LDs]) and compared it with the proteasome inhibitor Bortezomib treatment. SR9009-treated cells exhibited significant reduction in cell viability with consequences on cell cycle progression. Dexamethasone synchronized cells displayed differential time responses to SR9009 treatment with highest responses 18 to 30 h after synchronization. SR9009 treatment decreased ROS levels while Bortezomib increased them. However, both treatments significantly increased LD levels, whereas the combined treatment showed additive or synergistic effects between both drugs. In addition, we extended these studies to HepG2 cells which also showed a significant decrease in cell viability and ROS levels and the increase in LD levels after SR9009 treatment. Our results suggest that the pharmacological modulation of the tumor-intrinsic clock by REV-ERB agonists severely affects cell metabolism and promotes cytotoxic effects on cancer cells.

Keywords

tumor cell, glioblastoma, clock gene, redox state, lipid droplet, Bortezomib, REV-ERB

Received July 25, 2019; Revised October 29, 2019; Accepted for publication November 3, 2019

Introduction

Carcinogenesis is a complex and multi-etiological process resulting in the accumulation of genetic alterations primarily in genes involved in the regulation of signaling pathways relevant to the control of cell growth and division (reviewed in Hanahan and Weinberg, 2011). Neoplastic processes include a number of typical characteristics such as sustained proliferative activation, growth suppressor evasion, cell death resistance, replicative immortality, induction of angiogenesis, and invasiveness and metastasis, all of which are based on genome instability and inflammation.

Under physiological conditions, circadian clocks are near 24-h endogenous oscillators that control a complex net of physiological and behavioral processes such as the

daily sleep and wake cycle, body temperature, feeding behavior, hormone secretion, drug and xenobiotic metabolism, glucose homeostasis, and cell cycle progression (Lowrey and Takahashi, 2004; Bell-Pedersen et al., 2005). At the cellular level, a redox/metabolic oscillator

¹CIQUIBIC-CONICET, Facultad de Ciencias Químicas, Universidad Nacional de Córdoba, Córdoba, Argentina

²Departamento de Química Biológica “Ranwel Caputto,” Facultad de Ciencias Químicas, Universidad Nacional de Córdoba, Córdoba, Argentina

Corresponding Author:

Mario E. Guido, CIQUIBIC-CONICET, Facultad de Ciencias Químicas, Universidad Nacional de Córdoba, Haya de la Torre s/n, Ciudad Universitaria, 5000 Córdoba, Argentina.
Email: mguido@fcq.unc.edu.ar



(R/MO) has been described to interact with the circadian molecular clock (Dibner and Schibler, 2015; Wagner et al., 2018); this R/MO has been shown to be ancestral and highly conserved through evolution (review in Edgar et al., 2012). Taken together, we may infer that the cellular clock that temporarily controls cellular processes is made up of a molecular clock (transcription/translation feedback loop) and an R/MO. In mammals, disruption of circadian rhythms increases cancer incidence and metabolic disorders. Cell-autonomous clocks are composed of a transcription–translation-based feedback loop made up of a set of genes that include *Clock* (and its paralogue *Npas2*) and *Bmal1* as activator components and *Per1*, *Per2*, *Cry1*, and *Cry2* as repressor components (King et al., 1997; Gekakis et al., 1998). The entire cycle of transcription and translation takes approximately 24 h to be completed. In addition, the CLOCK–BMAL1 complex may activate a second alternative cycle involving the nuclear receptors REV-ERB α and REV-ERB β which compete at the retinoic acid-related orphan receptor (ROR)-binding elements with the activators ROR α , ROR β , and ROR γ (Preitner et al., 2002; Sato et al., 2004; Zhang et al., 2015). The rhythmic expression of REV-ERB α/β leads to the repression of BMAL1 and CLOCK, which in turn induces a rhythm in these genes that is in antiphase with period (PER) expression rhythms (Preitner et al., 2002). In fact, REV-ERBs and RORs are crucial components of the circadian clock that links the core circadian oscillator to the regulation of clock-controlled genes, which in turn regulate metabolic pathways and several physiological processes, including metabolism, development, and immunity. In consequence, loss-of-function studies both *in vitro* and *in vivo* support the REV-ERB key role in lipid metabolism, regulation of plasma glucose levels (Delezie et al., 2012; Solt et al., 2012), as well as the oxidative capacity of skeletal muscle and mitochondrial biogenesis (Woldt et al., 2013).

The development and characterization of pyrrole derivatives SR9009 and SR9011 (Solt et al., 2012) as specific REV-ERB agonists opened up the possibility of targeting these receptors to treat several circadian disorders, including metabolic diseases (obesity, dyslipidemia, and glucose intolerance; Green et al., 2008; Bass and Takahashi, 2010; Bass, 2012; Eckel-Mahan and Sassone-Corsi, 2013; Gamble and Young, 2013), sleep disorders (Solt et al., 2012) and cancer (Sulli et al., 2018). Indeed, pharmacological modulation of circadian rhythms by these agonists affects tumor cell viability by restraining pathways that are aberrantly activated in cancer (Sulli et al., 2018). Consistent with the range of metabolic effects noted in REV-ERB α -null mice, pharmacological activation of REV-ERB with SR9009 and SR9011 had additional metabolic effects in mice including weight loss in diet-induced obese mice, events associated with an increase in energy expenditure without

alterations in locomotor behavior or food intake (Solt et al., 2012). Taking into account the role of REV-ERBs on lipid, glucose, and energetic metabolism regulation and the high metabolic demands of cancer cells, we postulated that a pharmacological modulation of circadian components repressors such as REV-ERBs could alter metabolic pathways that compromise cancer cell survival.

Although disruption of the biological clock altering metabolic pathways can lead to diverse pathologies, little is known about the temporal regulation of cellular metabolism in tumor cells. Glioblastoma multiforme (GBM) is the most aggressive human brain tumor characterized by the aberrant proliferation growth of glial-like tumor cells. In this connection, the human glioblastoma T98G cells constitute an appropriate cancer cell model to investigate the tumor-intrinsic circadian clock. In our previous work, we found that proliferating T98G cells contain a functional intrinsic oscillator that controls diverse metabolic processes including lipid metabolism, levels of reactive oxygen species (ROS), peroxiredoxin oxidation cycles and susceptibility to treatment with the proteasome inhibitor Bortezomib (BOR; Wagner et al., 2018).

Here, we investigated the effects of SR9009 treatment in T98G cell cultures and compared it with BOR treatment assessing cell viability, differential time responses to chemotherapy after synchronization with dexamethasone (DEX), and metabolic processes involving ROS and lipid droplet (LD) levels. In addition, we extended these studies to HepG2 cells, a nonneuronal tumor cell line derived from human liver hepatocellular carcinoma.

Material and Methods

Cell Cultures

T98G cells are derived from the human GBM (ATCC, Cat. No. CRI-1690, RRUD: CVCL0556, Manassas, VA, USA) and tested positive for glial cell markers and negative for mycoplasma contamination. HepG2 cells (ATCC, Cat. No. HB-8065, RRID: CVCL0027) are derived from the human hepatocellular carcinoma. Both cell lines were grown in Dulbecco's modified Eagle's medium (DMEM) (Gibco, BRL, Invitrogen, Carlsbad, CA, USA) supplemented with 10% fetal bovine serum (FBS) according to (Portal et al., 2007) at 37°C and 5% CO₂.

SR9009 Treatment and Determination of Cell Viability by MTT Assay

Cells were plated in 96-well plates at a density of 1×10^4 and were allowed to attach overnight at 37°C. Cultured cells were incubated with DMSO (vehicle) or REV-ERB

agonist (SR9009) at different concentrations (10, 20, and 40 μM) and incubation time (24, 48, and 72 h). Stock solutions of SR9009 were resuspended in DMSO to a final concentration of 50 mM (stock solution) according to manufacturer's instructions. After incubation, 10 μL of 3-(4,5-dimethylthiazol-2-yl)-2,5-diphenyltetrazolium bromide (MTT) reagent (5 mg/mL; Sigma) were added to each well, and plates were further incubated for 2 h at 37°C as described (Vlachostergios et al., 2013). Then, 100 μL of DMSO:isopropanol (1:1, v/v) was added to each well followed by incubation for a few minutes at room temperature protected from light. Samples were analyzed at a wavelength of 570 nm with a reference at 650 nm in an Epoch Microplate Spectrophotometer. Vehicle-treated cells (DMSO) were considered as 100% of viability.

In other series of experiments, 5×10^3 HepG2 cells were allowed to attach overnight at 37°C in a 96-well plate. Cultured cells were incubated with DMSO (vehicle) or REV-ERB agonist (SR9009) at different concentrations (5, 10, 20, and 40 μM) for 96 h. Then, cell viability was analyzed by MTT assay considering vehicle-treated cells (DMSO) as 100% of viability.

SR9009 Treatment of T98G Cells and Determination of Cell Viability by alamarBlue Assay

Cells were plated in 96-well plates at the density of 1.5×10^3 and allowed to attach overnight at 37°C. Cultured cells were incubated with DMSO (vehicle) or REV-ERB agonist (SR9009) at final concentration of 20 μM for 48 or 72 h. After incubation, 10 μL of alamarBlue reagent (Invitrogen) were added to each well (final volume: 100 μL in 96-well plates) and plates were further incubated for 3 h at 37°C protected from light. Fluorescence intensity was analyzed at an excitation wavelength of 540 to 570 nm, and fluorescence emission reads at 580 to 610 nm in a Biotek microplate reader. Vehicle-treated cells (DMSO) were considered as 100% of viability.

Differential Temporal Susceptibility to SR9009 or BOR Treatment

T98G cells were plated in 96-well plates at the density of 1×10^4 and allowed to attach overnight in a CO₂ incubator at 37°C. Cell cultures were synchronized by a 20-min shock with 100 nM DEX and were treated with SR9009 (20 μM 48 h) or BOR (500 nM 36 h; Comba et al., 2019) at different times postsynchronization. After incubation, cell viability was determined by MTT assay as described earlier and analyzed at 570 nm with a reference at 650 nm in an Epoch Microplate Spectrophotometer. Vehicle-treated cells (DMSO) were considered as 100% of viability.

Combined Chemotherapeutic Treatments on T98G Cells

In other series of experiment, T98G cells were treated with both drugs together to evaluate the additive/synergistic effect between them. For this, T98G cells were synchronized by a 20 min shock with 100 nM DEX at 37°C and maintained in 5% FBS-DMEM. Cells were treated with different drug concentrations alone or in combination as follows: BOR (50 or 500 nM), SR9009 (10 or 20 μM), BOR (50 nM)+SR9009 (10 μM), or BOR (500 nM)+SR9009 (20 μM), 18 h postsynchronization, and were incubated for 36 h at 37°C. Cell viability was analyzed by MTT assay as described earlier. Vehicle-treated cells (DMSO) were considered as 100% of viability.

Cell Cycle Progression Analysis in SR9009-Treated T98G Cells

T98G cells incubated with DMSO (vehicle) or SR9009 (20 μM) were arrested in serum-free DMEM for 36 h. Then, the medium was removed and either vehicle or SR9009-treated cells were stimulated with 20% serum for 16 h in the presence of DMSO or SR9009, respectively. Finally, cells harvested by trypsinization were washed in cold phosphate buffered saline (PBS) and fixed with cold 70% ethanol at 20°C for at least 24 h. Cell pellets were resuspended in 150 μL of staining solution (PBS containing 50 $\mu\text{g}/\text{mL}$ propidium iodide and 10 μg RNase A) as reported (Acosta-Rodríguez et al., 2013). Cell cycle analysis was performed by a flow cytometer running at least 50,000 cells. The analysis program used was FlowJo software (Verity Software House, Topsham, ME, USA).

Redox State in SR9009-Treated Cells

Redox state was analyzed in T98G cells incubated with SR9009 (20 μM , 48 h) or BOR (500 nM, 24 h) and in SR9009-treated-HepG2 cells (40 μM , 48 h). Briefly, the culture medium was removed and cells were washed with cold PBS 1X and harvested by trypsinization. Then, cells were incubated with 2,7-dichlorodihydrofluorescein diacetate at 2 μM final concentration for 40 min at 37°C, washed twice with PBS 1X, and the fluorescence intensity was measured by flow cytometry at 530 nm when the sample was excited at 485 nm (Eruslanov and Kusmartsev, 2010). Cells without the fluorescent indicator were used as negative control, and propidium iodide (50 $\mu\text{g}/\text{mL}$) staining was used to discriminate viable cells. *FlowJo* software was used to analyze fluorescence intensity (Verity Software House).

Determination of LDs on Cells Treated With SR9009 or BOR

T98G cells were incubated with SR9009 (20 μ M, 48 h) or BOR (500 nM, 24 h), and LD levels were analyzed by confocal microscopy and flow cytometry. For microscopy visualization, cultured cells were fixed for 15 min in 4% paraformaldehyde in PBS and washed twice with PBS 1X. Then, cells were incubated with Nile Red (1 μ g/mL, Sigma, Tokyo, Japan) for 15 min at room temperature protected from light. Coverslips were finally washed thoroughly and visualized by confocal microscopy (FV1200; Olympus, Tokyo, Japan). Cellular nuclei were visualized by 4',6-diamidino-2-phenylindole (DAPI) staining. Average size quantification of LD was carried out with *ImageJ* software.

For flow cytometry analysis, either control or treated cells were harvested by trypsinization and washed twice with PBS 1X. Cell pellets were resuspended in 200 μ L of PBS containing 1 μ g/mL Nile Red and were incubated for 15 min at room temperature protected from light. Then, cells were washed twice with PBS 1X, and the fluorescence intensity was measured by flow cytometry (BD LSRFortessa™ cell analyzer) with 575/26 filter. A negative control including cells without the fluorescent indicator was used. FlowJo software was used to analyze fluorescence intensity.

HepG2 cells were treated with SR9009 (10 or 40 μ M, 96 h), and LD content was assessed by Nile Red (1 μ g/mL) staining as described earlier. Average size and area of LDs were performed by the *ImageJ* software. Cellular nuclei were visualized by DAPI staining.

Immunocytochemistry

Immunocytochemistry was performed as described (Morera et al., 2016). Briefly, cultured cells were fixed for 15 min in 4% paraformaldehyde in PBS and 10 min in methanol. Coverslips were washed in PBS, were treated with blocking buffer (PBS supplemented with 0.1% bovine serum albumin, 0.1% Tween 20, and 0.1% glycine) and were incubated overnight with primary antibodies (Table 1) at 4°C. Coverslips were washed 3 times and were incubated with goat antirabbit immunoglobulin G (IgG; Jackson 549 antibody 1:1,000) or goat antimouse IgG (Jackson 488 antibody 1:1,000) for 1 h at

room temperature. Coverslips were finally washed thoroughly and visualized by confocal microscopy (FV1200; Olympus). Cellular nuclei were visualized by DAPI staining.

Statistics

Statistical analyses involved a one- or two-way analysis of variance (ANOVA) to test the time or drug treatment effects and Kruskal–Wallis (K-W), the nonparametric one-way ANOVA or Scheirer–Ray–Hare test when the normality assumption of residuals was violated. Pairwise comparisons involved the Student *t* test, Bonferroni, or Dunn–Bonferroni post hoc when appropriate as stated in figure legends. For Scheirer–Ray–Hare test, all analyses were followed by K-W test with Bonferroni correction as post hoc analysis. Data are expressed as mean \pm standard error of the mean. In all cases, significance was considered at $p < .05$.

Results

Here, we investigated SR9009 effects and compared it with BOR, a proteasome inhibitor previously used, on T98G cell viability, differential chemotherapy time responses, and underlying metabolic processes concerning ROS and LD levels. Also, we extended these studies to HepG2 cells to evaluate the SR9009 effects on cell viability, LD, and ROS levels.

Characterization of T98G Cells and Susceptibility to SR9009 Treatment

Human T98G cells kept in culture under proliferative conditions (5% FBS-DMEM) expressed typical markers for glial cells such as vimentin, glutamine synthase, and glial fibrillary acidic protein (Figure 1(a) to (c)) as well as the circadian clock component REV-ERB α (Figure 1(d)). In addition, T98G cells were previously shown to express the clock protein PER1 and display temporal fluctuations on PER1-like protein by immunocytochemistry with highest levels at 18 and 24 h after synchronization (Wagner et al., 2018).

When cells were treated with the REV-ERB-specific agonist SR9009 at different concentrations going from 10 to 40 μ M for 24, 48, or 72 h (Figures 1 and 2(a)),

Table 1. Antibody List.

Antibody	Host	Catalogue	Dilution
Glutamine synthase	Mouse	Millipore Cat# MAB302, RID:AB_2110656	1:100
Vimentin	Mouse	Sigma-Aldrich Cat# V5255, RRID:AB_477625	1:750
GFAP	Rabbit	Agilent Cat# Z0334, RRID:AB_10013382	1:250
REV-ERB α	Mouse	Santa Cruz Biotechnology Cat# sc-100910, RRID:AB_2154647	1:100

Note. Summary of antibodies used indicating antibody name, host, catalogue number, and dilution for immunochemistry. GFAP = glial fibrillary acidic protein.

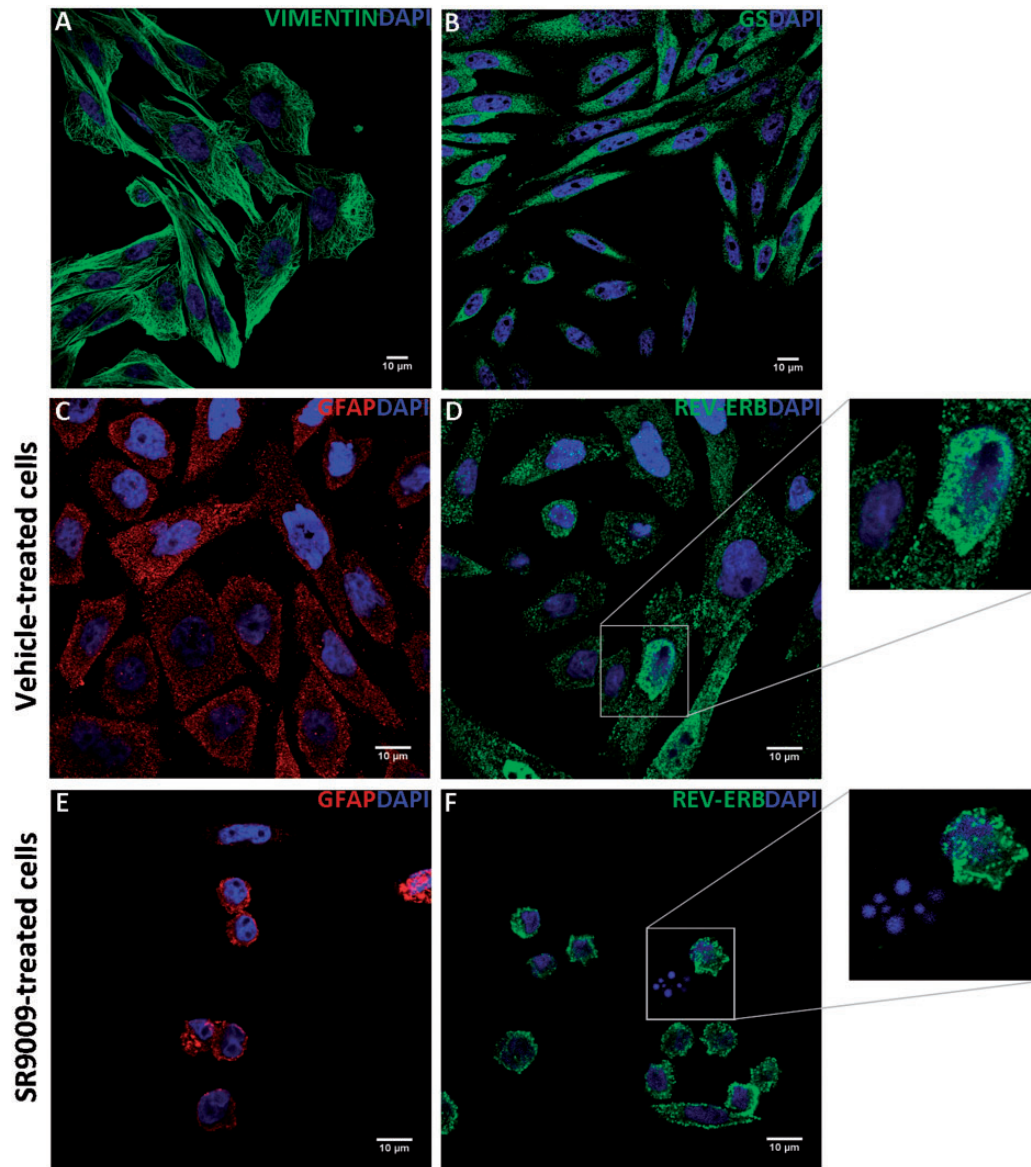


Figure 1. Protein expression in T98G cells by immunocytochemistry and SR9009 treatment effect. T98G cells express typical markers of glial cells such as vimentin (a—green) and GS (b—green) visualized by immunofluorescence with specific primary antibodies and confocal microscopy. T98G cells were incubated with vehicle (DMSO) or SR9009 (20 μ M) for 48 h and immunolabeled for GFAP (c and e—red) or REV-ERB α (d and f—green) with specific primary antibodies and confocal microscopy; insets on the right further magnified a single cell in both conditions (DMSO and SR9009 treatment). See “Materials and Methods” section for further detail. Scale bar = 10 μ m. GFAP = glial fibrillary acidic protein; GS = glutamine synthase.

significant effects on cell morphology (Figure 1(e) and (f)) and reduction in cell viability were observed at final concentrations of 20 and 40 μ M for 48 and 72 h (Figure 2(a)) as compared with vehicle-treated controls ($p < .0001$ by K-W). It is noteworthy that a significant decrease in cell viability is observed after SR9009 treatment with only approximately 20% of cells remaining viable under the tested conditions (20 and 40 μ M of SR9009 for 72 h). Moreover, a significant reduction in cell viability was also observed on SR9009-treated HepG2 cells (40 μ M for 96 h; $p < .0002$ by K-W;

Figure 2(b)). Nevertheless, although hepatic tumor cells seemed to be more resistant to chemotherapy because higher drug concentrations and longer treatment durations were required to cause less than 25% of cell survival (40 μ M for 96 h), we cannot discard any significant drug effect in cell viability at earlier times in combination with a higher drug concentration.

In addition, to further support these observations, cell viability was also analyzed by alamarBlue assay after T98G cells incubation with SR9009 (20 μ M) for 48 or 72 h at 37°C. Similar to findings found for MTT assay,

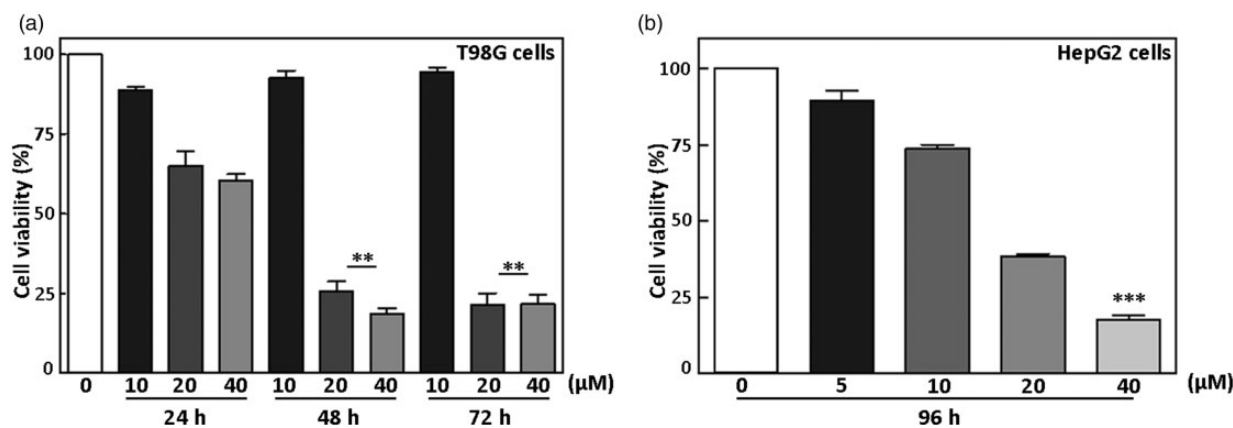


Figure 2. Cell susceptibility to SR9009 treatment in cultures of T98G (a) and HepG2 (b) cells. (a) T98G cells were treated with different SR9009 concentrations (10, 20, and 40 μM) for 24, 48, or 72 h at 37°C. Cell viability that was analyzed by MTT assay revealed a significant effect of SR9009 concentration ($p < .001$) and duration of treatment ($p < .05$) but not of interaction by Scheirer–Ray–Hare test. Post hoc comparisons revealed that viability of T98G cells incubated with a final concentration of 10 μM of SR9009 differed from values of cells treated with 20 or 40 μM (** $p < .017$) while 24 h of treatment differed from those at 48 h or 72 h (** $p < .017$). The results are mean \pm standard error of the mean of two independent experiments ($n = 5\text{--}6/\text{group}$). (b) HepG2 cells were treated with different SR9009 concentrations (5, 10, 20, and 40 μM) for 96 h. A significant reduction in cell viability was observed when HepG2 cells were treated with 40 μM for 96 h as compared with untreated cells (** $p < .0002$ by K-W). The results are mean \pm standard error of the mean of two independent experiments ($n = 5\text{--}6/\text{group}$).

a significant reduction in cell viability was observed when cells were treated with SR9009 (20 μM) for 48 or 72 h ($p < .0005$ by ANOVA; Supplementary Figure 1).

Differential Temporal Susceptibility to SR9009 Treatment

T98G cells were synchronized with DEX (100 nM) and were treated with SR9009 (20 μM) for 48 h at different times postsynchronization along 36 h. Cell viability was analyzed by MTT assay in SR9009-treated cells, and showed a significant temporal effect of drug treatment, with the lowest levels of viability during a time window going from 18 to 30 h after synchronization. The statistical analysis clearly revealed a significant effect of treatment versus time ($p < .0041$ by K-W; Figure 3(a)). These observations agree with those previously found in synchronized T98G cells treated with BOR (500 nM) for 36 h (Wagner et al., 2018) exhibiting the lowest cell viability in a time window going from 12 to 24 h postsynchronization ($p < .0007$ by K-W; Figure 3(b)).

Effects of Cell Cycle Progression of SR9009 Treatment on T98G Cells

To further investigate whether SR9009 treatment alters cell cycle progression, T98G cells were arrested in serum-free medium for 36 h in the presence of DMSO (vehicle) or SR9009 (20 μM). Then, medium was removed and either control or treated cells were stimulated with 20% serum for 16 h in the presence of DMSO or SR9009 respectively. Flow cytometry analysis showed a higher

proportion of SR9009-treated cells (~58%) in G_0/G_1 phases after serum stimulation as compared with vehicle-treated cells (~43%; $p < .0053$ by t test). By contrast, vehicle-treated cells showed a higher proportion of cells in S phase (~40%) with respect to SR9009-treated cells (~22%; $p < .0121$ by t test; Figure 4(a) to (c)).

SR9009 Effect on Redox and Lipid Metabolism

To investigate whether oxidative stress could be involved in the effects of SR9009 treatment in cell viability, we analyzed ROS levels and compared it with those in BOR-treated cells. To this end, T98G cells were incubated with SR9009 (20 μM) for 48 h, and the redox state was analyzed by incubation with 2',7'-dichlorodihydrofluorescein diacetate (2 μM) for 40 min at 37°C. When fluorescence intensity was measured by flow cytometry, a significant reduction in ROS levels was seen in SR9009-treated cells as compared with vehicle-treated controls ($p < .007$ by t test; Figure 5(a)). In contrast, T98G cells previously incubated with BOR (500 nM) for 24 h showed higher levels of ROS with respect to those in control cells ($p < .04$ by t test; Figure 5(b)). Moreover, SR9009 (40 μM) treatment in HepG2 cells for 96 h also showed a significant decreased on ROS levels as compared with vehicle-treated cells ($p < .0001$ by ANOVA; Figure 7(f)).

Figure 5.

In other series of experiments, we proceeded to evaluate the LD levels after treatments with SR9009 or BOR. LDs are cytoplasmic organelles responsible for storing the excess of cellular lipids (Farese and Walther, 2009;

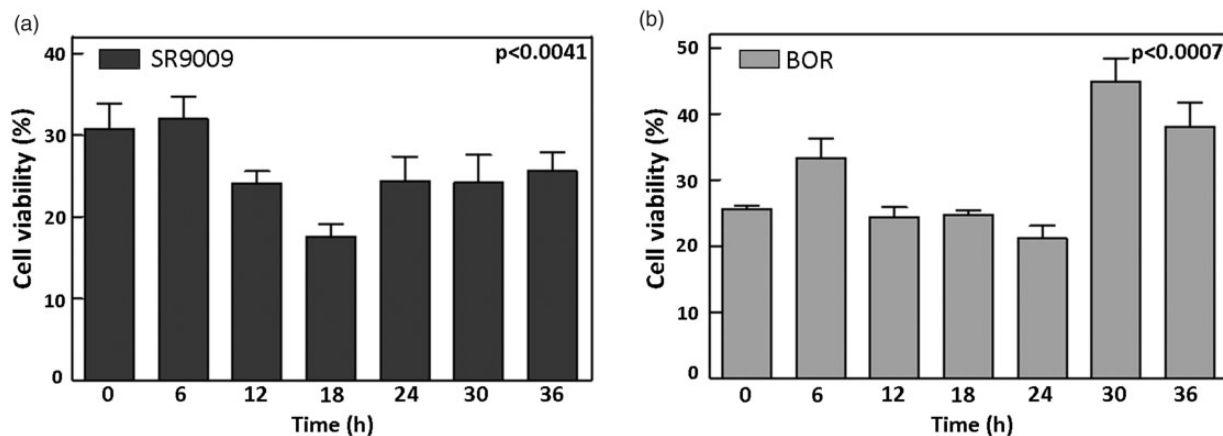


Figure 3. Temporal response to SR9009 (a) or BOR (b) treatment in T98G cells. (a) Cells were synchronized with DEX (100 nM), and SR9009 was added to a final concentration of 20 μ M at different times postsynchronization for 48 h. Cell viability was analyzed by MTT assay as described in “Materials and Methods” section. A significant temporal variation was observed in levels of T98G cell viability ($p < .004$ by K-W). Pairwise comparisons by Dunn–Bonferroni post hoc revealed that the treatment beginning at 6 h post synchronization significantly differed from those starting at 18, 24, and 30 h after synchronization. The results are mean \pm standard error of the mean of three independent experiments ($n = 5\text{--}6/\text{group}$). (b) DEX-synchronized cells were treated with BOR (500 nM) for 36 h at different times postsynchronization and cell viability assessed by MTT assay. A significant time effect was observed in levels of T98G cell viability ($p < .0007$ by K-W) as previously observed in Wagner et al. (2018). Results are mean \pm standard error of the mean from one representative experiment ($n = 5\text{--}6/\text{group}$). BOR = Bortezomib.

Beller et al., 2010; Brasaemle and Wolins, 2012) and mainly involved in energy storage.

To investigate whether SR9009 treatment alters lipid accumulation in LDs, we used Nile Red which is intensely fluorescent and can serve as a sensitive vital stain for the detection of cytoplasmic LDs. To this end, SR9009 or BOR-treated cells were stained with Nile Red and LDs visualized by confocal microscopy and flow cytometry. First, LDs in SR9009-treated cells showed a higher average size as compared with vehicle-treated cells ($p < .003$ by t test; Figure 6(a) to (c)). In agreement with this, a higher fluorescence intensity was visualized by flow cytometry either in SR9009 or BOR-treated cells as compared with untreated cells ($p < .002$ and $p < .025$, respectively, by t test; Figure 6(d) to (f)).

Similar results were observed in HepG2 cells exhibiting a higher average size of LDs after SR9009 treatment (10 and 40 μ M, 96 h) as compared with control cells ($p < .0001$ by ANOVA; Figure 7(a) to (d)). Moreover, the percentage of LD area related to the total area of each cell was increased after drug treatment (40 μ M, 96 h; Figure 7(e); $p < .0001$ by K-W).

Combined Chemotherapeutic Treatments on T98G Cells

Even though SR9009 or BOR treatments showed marked effects in cell viability, we explored whether the combination of these two drugs could improve chemotherapeutic effects. To this end, T98G cells were treated with BOR (50 or 500 nM), SR9009 (10 or 20 μ M), and their

combination (BOR 50 nM + SR9009 10 μ M or BOR 500 nM + SR9009 20 μ M) at 18 h postsynchronization for 36 h, and cell viability was analyzed by MTT assay. When BOR or SR9009 treatments were given alone at low doses, a 60% of cells still remained viable; however, the combination of these compounds at low concentrations (BOR 50 nM + SR9009 10 μ M) reduced cell viability to 28% (Figure 8(a)) as compared with each drug alone ($p < .003$ by K-W). In addition, at high drug concentration, 28% and 34% of cells remained viable, after BOR or SR9009 treatment, respectively; whereas, when both drugs were applied together to T98G cells at high doses, a significant reduction in cell viability was observed and only 17% of cells were still viable ($p < .0001$ by ANOVA; Figure 8(b)). The results clearly demonstrated an important additive or synergistic effect of drug combination.

Discussion

Our results demonstrated that the pharmacological modulation of tumor-intrinsic clock components by a specific REV-ERB agonist severely affected tumor cell metabolism and promoted cytotoxic effects on glioma and hepatocellular carcinoma cells. These observations showed for the first time that glioblastoma cells can be treated pharmacologically under a time-dependent therapy through the modulation of particular circadian clock components such as REV-ERBs involving the control of metabolism to achieve the highest antitumor treatment efficacy. SR9009 treatment altered the typical glial cell

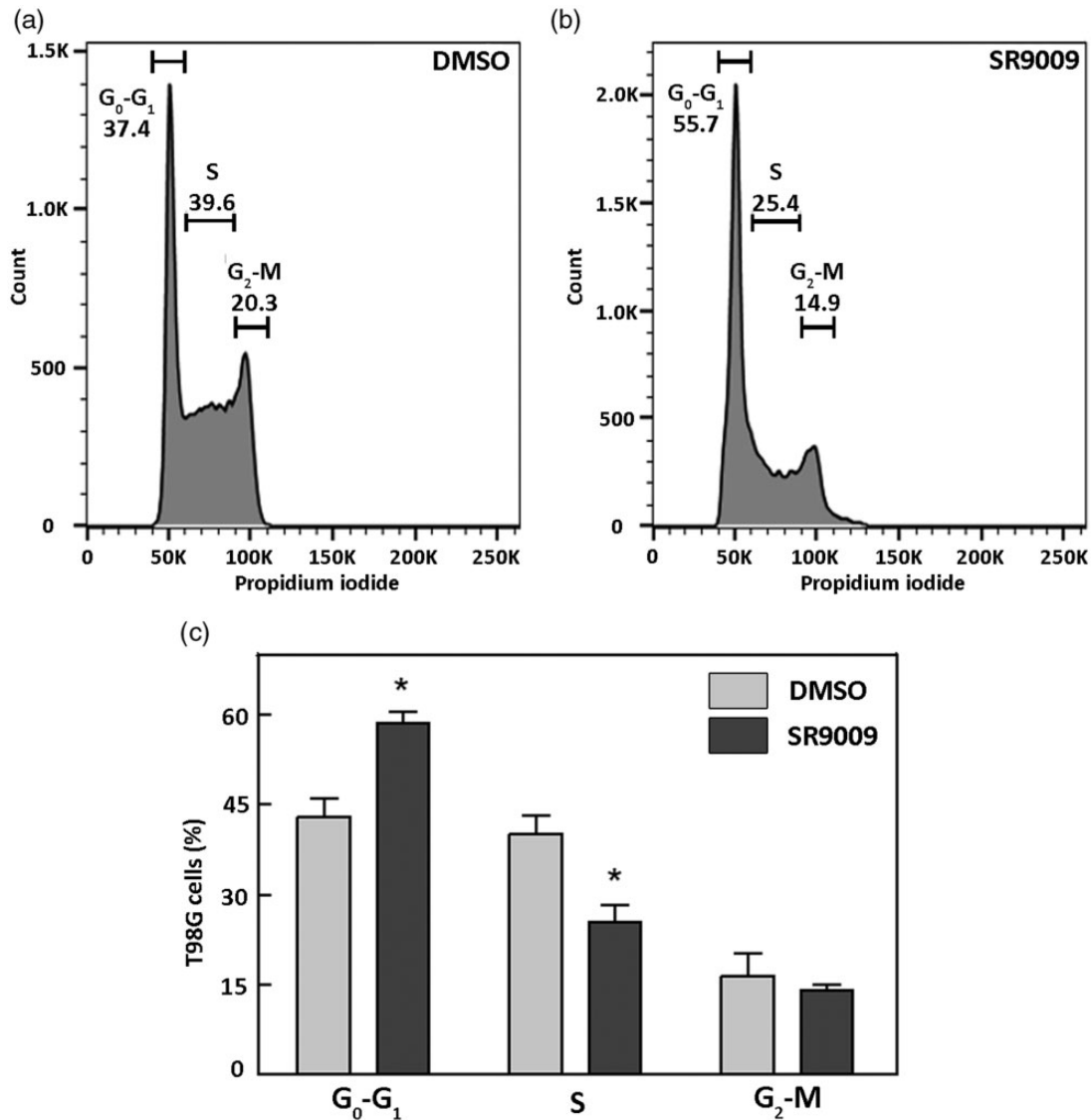


Figure 4. Effects of SR9009 treatment on cell cycle distribution of T98G cells. T98G cells incubated with DMSO (vehicle) or SR9009 (20 μ M) were arrested in serum-free DMEM for 36 h. Then, the medium was removed and either vehicle or treated cells were stimulated with 20% fetal bovine serum for 16 h in the presence of DMSO or SR9009 as appropriate. Cell cycle phases were analyzed by staining with propidium iodide and flow cytometry. Representative cell cycle distributions are shown in control (a) or SR9009-treated cells (b). (c) Quantification of the percentage of cells in each phase showed a higher proportion of SR9009-treated T98G cells in G₀-G₁ phase (G₀-G₁ * p < .0053, S * p < .01 by t test). The results are mean \pm standard error of the mean of three independent experiments ($n = 4$ /group).

morphology (Figure 1), cell viability (Figures 2 and 3), and metabolism by increasing levels of LDs and decreasing those for ROS (Figures 5 and 6). Moreover, the treatment with SR9009 further potentiates the effect of BOR (Figure 8), which was previously shown to have strong effects on cell viability of glioma cells under a circadian chronotherapy (Wagner et al., 2018). However, the mechanisms used for these two chemotherapeutic agents seemed to be different in terms that BOR inhibits the proteasome function while SR9009 acts on the clock-related cellular metabolism; nevertheless, both of them were shown to substantially elevate levels of LDs

(Figures 6 and 7). Also, and remarkably, both agents exhibited a clear time window of highest cellular susceptibility to treatment with maximal effects from 12–18 to 24 h after DEX synchronization (Figure 3 and Wagner et al., 2018). Moreover, when the circadian clock was disturbed by *Bmal1* knock-down, a circadian variation in BOR treatment susceptibility was still observed but with a different phase and amplitude than that described in wild-type T98G cells (Wagner et al., 2018). In previous reports, proliferative T98G cells were synchronized by DEX which is commonly used in GBM patients to reduce inflammation or as a chemotherapy adjuvant; in

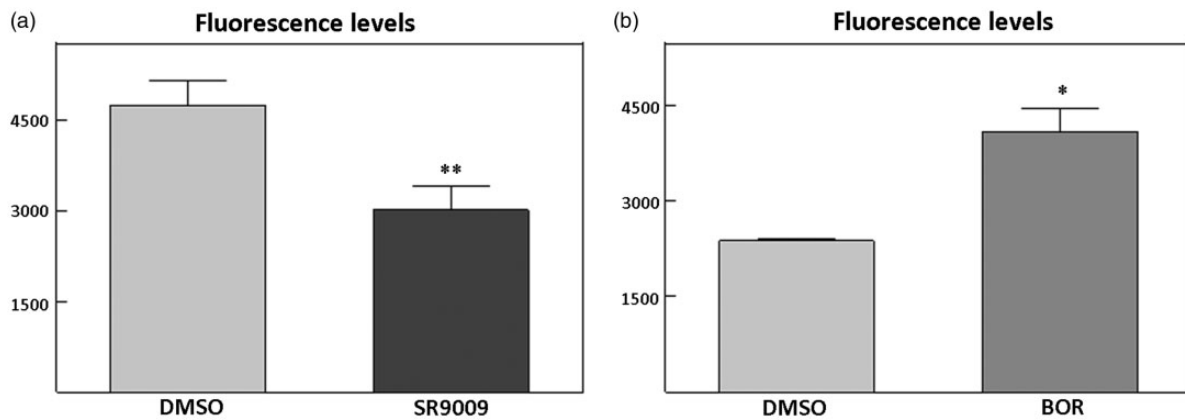


Figure 5. ROS levels in T98G cells treated with SR9009 or BOR. T98G cells were treated either with SR9009 (a, 20 μ M 48 h) or BOR (b, 500 nM 24 h), and ROS levels were analyzed with the fluorescent probe 2,7-dichlorodihydrofluorescein diacetate to a final concentration of 2 μ M as described in “Materials and Methods” section. Fluorescence intensity was analyzed by flow cytometry. The results are mean \pm standard error of the mean of two/three independent experiments ($n = 3\text{--}5/\text{group}$). The statistical analysis revealed a significant effect for SR9009 (** $p < .001$ by t test) and for BOR (* $p < .04$ by t test) as compared with vehicle-treated controls. BOR = Bortezomib.

fact, glucocorticoids can inhibit cancer cell proliferation by limiting the number of cells in S phase and additionally increasing the time spent in the G_1 phase (Kiessling et al., 2017; Wagner et al., 2018).

Results shown in Figure 4 strongly indicate that this REV-ERB agonist also affected the cell cycle progression because approximately 60% of SR9009-treated cells remained arrested in G_0/G_1 phases as compared with control cells after serum stimulation. It is known that GBM is the most aggressive brain tumor and that the development of more effective anticancer strategies can be useful for clinical use. In this regard, the combination of both agents applied at the right temporal window and at lower individual doses as seen in glioma cell cultures can offer an additional opportunity to effectively treat cancer cells in a synergic manner.

Circadian rhythms are intricately linked to the regulation of metabolism, and genetic perturbations of core clock genes lead to a range of abnormal metabolic phenotypes in mice, including obesity, dyslipidemia, and glucose intolerance (Green et al., 2008; Bass and Takahashi, 2010; Bass, 2012; Eckel-Mahan and Sassone-Corsi, 2013; Gamble and Young, 2013). In this connection, modern life including hypercaloric diets, sedentary routines, artificial illumination at night, the reduction in sleep hours, shiftwork, and jetlag among others may cause circadian disorganization promoting higher cancer risk and metabolic disorders.

RORs and REV-ERBs play key roles in the regulation of metabolic pathways linking the core circadian oscillator to the regulation of clock-controlled genes. Loss-of-function studies both *in vitro* and *in vivo* demonstrate that REV-ERBs have a crucial role in lipid metabolism as seen in REV-ERB α -null mice exhibiting

dyslipidemia with elevated levels of very-low-density lipoprotein, triglyceride, and increased serum levels of apolipoprotein C3 (Raspé et al., 2001, 2002). In this connection, lipids are stored in LDs as neutral lipids, namely, free fatty acids and cholesterol that are enzymatically converted to triacylglycerol and cholesteryl esters, respectively, and then incorporated into LDs (Farese and Walther, 2009; Beller et al., 2010; Brasaemle and Wolins, 2012). These organelles are not only restricted to energy storage but also participate in stress protection, protein sequestration, membrane trafficking, and signaling having a great impact on physiology, health, and disease (Welte and Gould, 2017). Nevertheless, the treatment with SR9009 significantly increased average size of LDs in T98G as well as in HepG2 cells. These observations agreed with a significant deficiency in surfactant phospholipids such as phosphatidylcholine or accumulation of phosphatidic acid under SR9009 treatment increasing LD fusion or coalescence (Guo et al., 2008; Fei et al., 2011). In fact, REV-ERB agonists were shown to be inhibitors of autophagy and *de novo* lipogenesis, with selective activity toward malignant and benign neoplasms; the accumulation of LDs may be due to an uptake and accumulation of fatty acids (Bensaad et al., 2014) and not to *de novo* synthesis of lipids as the expression of the two key enzymes fatty acid synthase and stearoyl-CoA desaturase 1 involved in *de novo* lipogenesis were decreased after REV-ERBs agonist treatment (Sulli et al., 2018).

Interestingly, autophagy contributes to the intracellular catabolism of lipids in hepatocytes, fibroblasts (Singh et al., 2009), and neurons (Martinez-Vicente et al., 2010), while the pharmacologic or genetic inhibition of

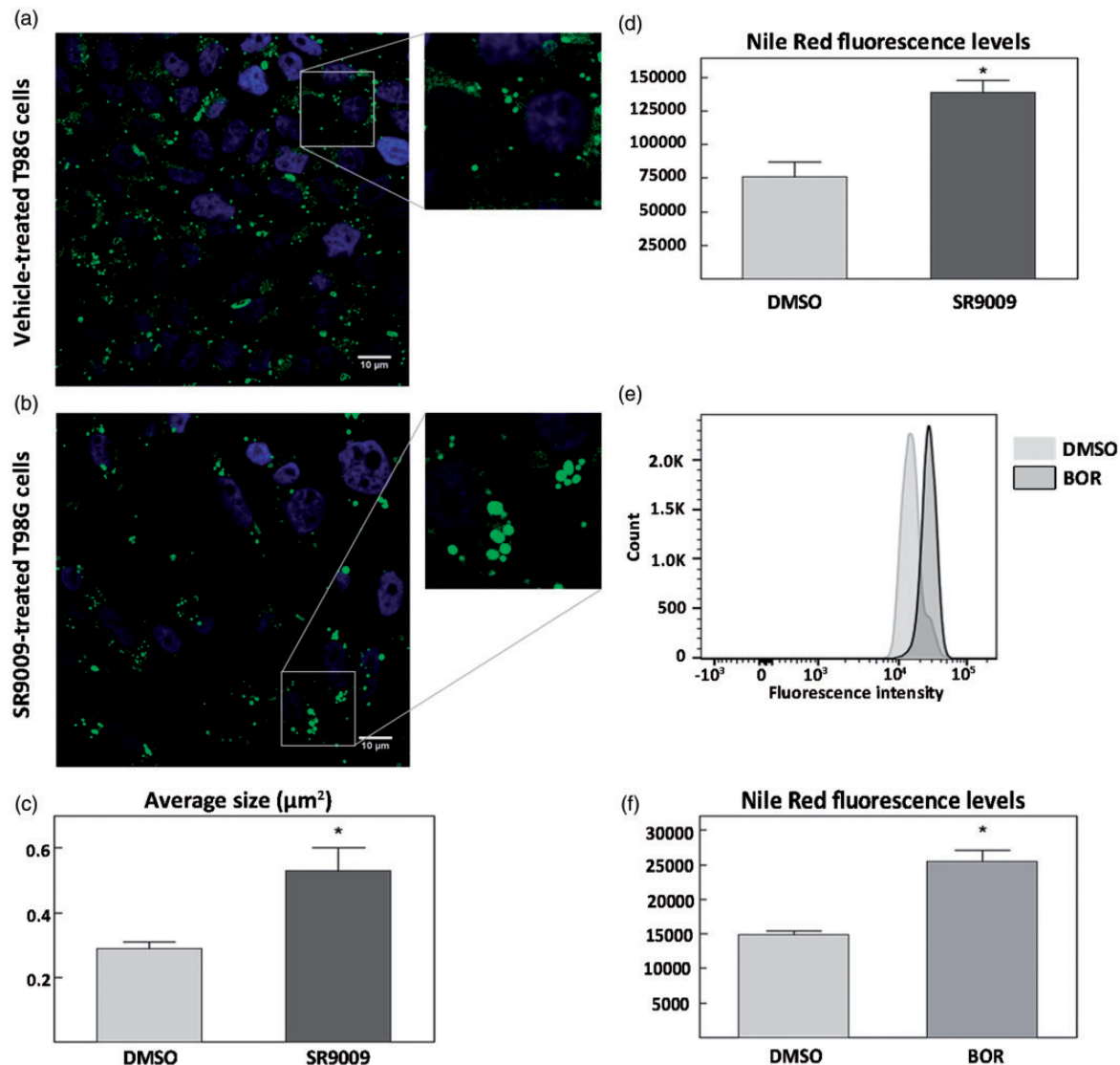


Figure 6. Lipid droplet (LD) levels in T98G cells treated with SR9009 or BOR. T98G cells were treated either with SR9009 (20 μM , 48 h; a to d) or BOR (500 nM, 24 h; e to f) and LD levels were analyzed by Nile Red staining. Representative microphotography of LDs observed in vehicle (a) or SR9009-treated T98G cells (b) stained with Nile Red were visualized by confocal microscopy, further magnified in the insets on the right. Scale bar = 10 μm . (c) Bar graphs showing quantification of average size of LDs in SR9009-treated T98G cells. Results revealed a higher average size of LDs in cells treated with SR9009 ($*p < .003$ by *t* test) as compared with controls. (d and f) Bar graphs showing quantification of fluorescence intensity of LDs stained with Nile Red and analyzed by flow cytometry. In both treatments, results showed a higher fluorescence intensity when T98G cells were treated with SR9009 (d, $*p < .002$ by *t* test) or BOR (f, $*p < .025$ by *t* test) as compared with controls. (e) Representative histograms of fluorescence intensity of LDs were analyzed by flow cytometry in BOR-treated cells. Data are mean \pm standard error of the mean. The results are mean of three independent experiments ($n = 3\text{--}5/\text{group}$). BOR = Bortezomib.

autophagy in hepatocytes leads to reduced rates of β oxidation and marked lipid accumulation in cytosolic LDs (Singh et al., 2009). Autophagy is an ATP-dependent process (Meijer and Codogno, 2004), and autophagy inhibition reduces mitochondrial β -oxidation rates (Singh et al., 2009; Heaton et al., 2010) and energy production. Autophagy-deficient stellate cells as shown in hepatocytes may be unable to process LDs by acid

lipases, resulting in LD accumulation and decreased free fatty acid availability, leading to decreased mitochondrial β oxidation.

Moreover, BOR treatment at low concentrations (5 nM) was shown to cause lipid accumulation associated with mitochondrial impairment (Guglielmi et al., 2017). The mechanisms used for these two chemotherapeutic agents seemed to be different concerning the redox

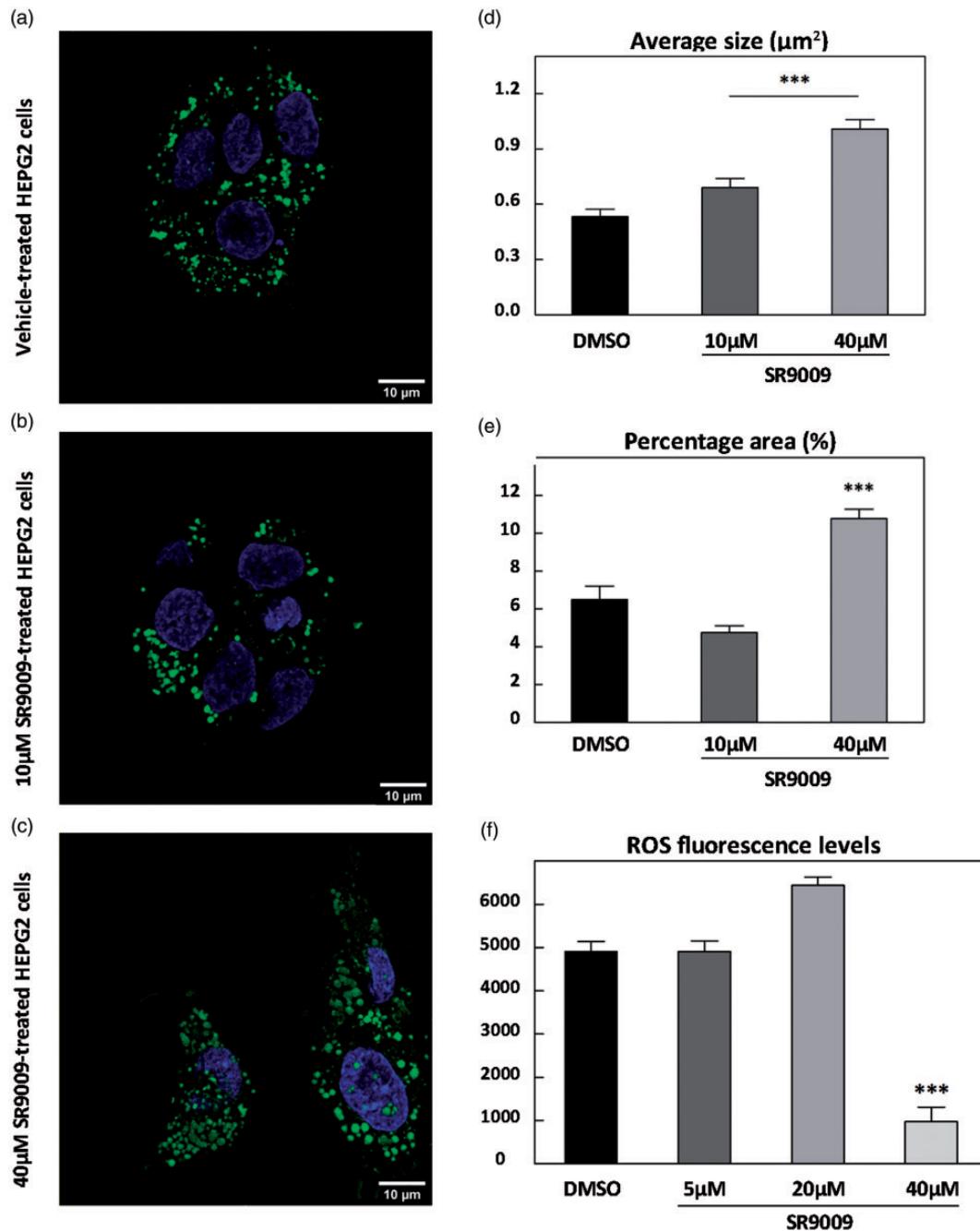


Figure 7. Lipid droplets (LDs) and ROS levels in HepG2 cells treated with SR9009. (a to c) Representative microphotographs of Nile Red-stained LDs in HepG2 cells treated with the vehicle (a) or SR9009 (b, 10 μM ; c, 40 μM). Scale bar = 10 μm . (d) Bar graph showing quantification of LD average size in SR9009-treated HepG2 cells that revealed a significant increase as compared with controls ($^{***}p < .0001$ by ANOVA, Bonferroni post hoc). (e) Bar graph showing quantification of LD percentage area in SR9009-treated HepG2 cells. A significant increase was observed with 40 μM SR9009 treatment for 96 h ($^{***}p < .0001$ by K-W). (f) Determination of ROS levels by flow cytometry in HepG2 cells treated with SR9009 (5 and 40 μM for 96 h). A significant reduction was observed at 40 μM SR9009-treated cells as compared with vehicle and 5 and 20 μM of SR9009 ($^{***}p < .0001$ by ANOVA, Bonferroni post hoc). ROS = reactive oxygen species.

state because BOR induced ROS levels while SR9009-treated cells showed decreased levels of them. Even though the sequence of events leading to apoptosis following proteasome inhibition by BOR is unclear, by-products of normal cellular oxidative processes such as

ROS have been suggested as regulating the process involved in the initiation of apoptotic signaling. Tan et al. (1998) previously showed that an increase in ROS generation induces cytochrome c release from mitochondria. Increased levels of ROS in BOR-treated cells

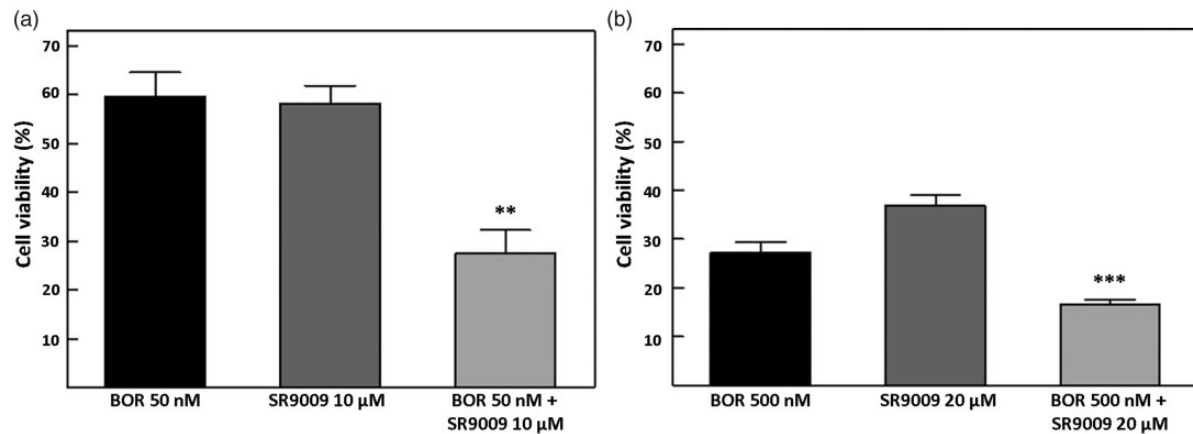


Figure 8. T98G cell susceptibility to the combined treatment with SR9009 and BOR. T98G cells were treated with BOR (50 or 500 nM), SR9009 (10 or 20 μM) and their combination (BOR 50 nM + SR9009 10 μM or BOR 500 nM + SR9009 20 μM) at 18 h postsynchronization for 36 h. Cell viability was analyzed by MTT assay and results showed a significant reduction in cell viability when T98G cells were treated with the combination of drugs (BOR 50 nM + SR9009 10 μM $**p < .003$, BOR 500 nM + SR9009 20 μM $***p < .0001$ by K-W) as compared with cells treated with each drug alone. Data are mean \pm standard error. The results are mean of three independent experiments ($n = 5-6$ /group). BOR = Bortezomib.

were also observed in colorectal (Kim, 2012) and human H460 nonsmall cell lung cancer cells (Ling et al., 2003) as well as in human leukemia cells (Yu et al., 2004). Conversely, SR9009-treated cells showed decreased ROS levels as compared with untreated cells for both tumor cell lines. These results support the idea proposed by Sulli et al. (2018) suggesting that excessive ROS production is not involved in the enhanced sensitivity of cancer cells to SR9009 treatment.

Overall, the pharmacological activation of REV-ERBs by the pyrrole derivative SR9009 as specific agonist (Solt et al., 2012) has been clearly shown to affect tumor cell viability restricting abnormally activated pathways as demonstrated on different tumor cell types, namely, brain, leukemia, breast, colon, and melanoma (Sulli et al., 2018). Therefore, and in agreement with these previously reported observations, the antitumor activity of SR9009 was clearly evidenced in T98G and HepG2 cells displaying significant cytotoxic effects and pronounced metabolic changes.

Summary

T98G cells constitute a glioblastoma model to evaluate the pharmacological modulation of tumor-intrinsic circadian clock components as anticancer strategies. Pyrrole derivatives (SR9009) acting as specific REV-ERBs agonists (circadian clock repressors) displayed potent in vitro activity on cancer cell metabolism and viability.

Acknowledgments

Authors are grateful to Mrs. Susana Deza, Gabriela Schanner and Dr. Carlos Mas for their excellent technical support and to Dr. Cesar Pucca for experimental advice.

Declaration of Conflicting Interests

The author(s) declared no potential conflicts of interest with respect to the research, authorship, and/or publication of this article.

Funding

The author(s) disclosed receipt of the following financial support for the research, authorship, and/or publication of this article: This work has been supported by Agencia Nacional de Promoción Científica y Técnica (FONCyT, PICT 2017 No 631), Consejo Nacional de Investigaciones Científicas y Tecnológicas de la República Argentina (CONICET) (PIP 2014) and Secretaría de Ciencia y Tecnología de la Universidad Nacional de Córdoba (SeCyT-UNC).

ORCID iD

Mario E. Guido  <https://orcid.org/0000-0002-5485-4904>

Supplemental Material

Supplemental material for this article is available online.

References

- Acosta-Rodríguez, V. A., Márquez, S., Salvador, G. A., Pasquaré, S. J., Gorné, L. D., Garbarino-Pico, E., Giusto, N. M., & Guido, M. E. (2013). Daily rhythms of glycerophospholipid synthesis in fibroblast cultures involve differential enzyme contributions. *J Lipid Res*, *54*(7), 1798–1811. doi:10.1194/jlr.M034264
- Bass, J. (2012). Circadian topology of metabolism. *Nature*, *491*(7424), 348–356. doi:10.1038/nature11704
- Bass, J., & Takahashi, J. S. (2010). Circadian integration of metabolism and energetics. *Science*, *330*(6009), 1349–1354. doi:10.1126/science.1195027

- Beller, M., Thiel, K., Thul, P. J., & Jäckle, H. (2010). Lipid droplets: A dynamic organelle moves into focus. *FEBS Lett*, *584*(11), 2176–2182. doi:10.1016/j.febslet.2010.03.022
- Bell-Pedersen, D., Cassone, V. M., Earnest, D. J., Golden, S. S., Hardin, P. E., Thomas, T. L., & Zoran, M. J. (2005). Circadian rhythms from multiple oscillators: Lessons from diverse organisms. *Nat Rev Gen*, *6*(7), 544–556. doi:10.1038/nrg1633
- Bensaad, K., Favaro, E., Lewis, C. A., Peck, B., Lord, S., Collins, J. M., Pinnick, K. E., Wigfield, S., Buffa, F. M., Li, J. L., & Zhang, Q. (2014). Fatty acid uptake and lipid storage induced by HIF-1 α contribute to cell growth and survival after hypoxia-reoxygenation. *Cell Rep*, *9*(1), 349–365. doi:10.1016/j.celrep.2014.08.056
- Brasaemle, D. L., & Wolins, N. E. (2012). Packaging of fat: An Evolving model of lipid droplet assembly and expansion. *J Biol Chem*, *287*(4), 2273–2279. doi:10.1074/jbc.R111.309088
- Comba, A., Bonnet, L. V., Goitea, V. E., Hallak, M. E., & Galiano, M. R. (2019). Arginylated calreticulin increases apoptotic response induced by Bortezomib in glioma cells. *Mol Neurobiol*, *56*(3), 1653–1664. doi:10.1007/s12035-018-1182-x
- Delezie, J., Dumont, S., Dardente, H., Oudart, H., Gréchez-Cassiau, A., Klosen, P., Teboul, M., Delaunay, F., Pévet, P., & Challet, E. (2012). The nuclear receptor REV-ERB α is required for the daily balance of carbohydrate and lipid metabolism. *FASEB J*, *26*(8), 3321–3335. doi:10.1096/fj.12-208751
- Dibner, C., & Schibler, U. (2015). Circadian timing of metabolism in animal models and humans. *J Intern Med*, *277*(5), 513–527. doi:10.1111/joim.12347
- Eckel-Mahan, K., & Sassone-Corsi, P. (2013). Metabolism and the circadian clock converge. *Physiol Rev*, *93*(1), 107–135. doi:10.1152/physrev.00016.2012
- Edgar, R. S., Green, E. W., Zhao, Y., van Ooijen, G., Olmedo, M., Qin, X., Xu, Y., Pan, M., Valekunja, U. K., Feeney, K. A., & Maywood, E. S. (2012). Peroxiredoxins are conserved markers of circadian rhythms. *Nature*, *485*, 459. doi:10.1038/nature11088
- Eruslanov, E., & Kusmartsev, S. (2010). Identification of ROS using oxidized DCFDA and flow-cytometry. *Methods Mol Biol*, *594*, 57–72. doi:10.1007/978-1-60761-411-1_4
- Farese, R. V., & Walther, T. C. (2009). Lipid droplets finally get a little R-E-S-P-E-C-T. *Cell*, *139*(5), 855–860. doi:10.1016/j.cell.2009.11.005
- Fei, W., Shui, G., Zhang, Y., Kraemer, N., Ferguson, C., Kapterian, T. S., Lin, R. C., Dawes, I. W., Brown, A. J., Li, P., & Huang, X. (2011). A role for phosphatidic acid in the formation of “supersized” lipid droplets. *PLoS Gen*, *7*(7), e1002201. doi:10.1371/journal.pgen.1002201
- Gamble, K. L., & Young, M. E. (2013). Metabolism as an integral cog in the mammalian circadian clockwork. *Crit Rev Biochem Mol Biol*, *48*(4), 317–331. doi:10.3109/10409238.2013.786672
- Gekakis, N., Staknis, D., Nguyen, H. B., Davis, F. C., Wilsbacher, L. D., King, D. P., Takahashi, J. S., & Weitz, C. J. (1998). Role of the CLOCK protein in the mammalian circadian mechanism. *Science*, *280*(5369), 1564–1569. doi:10.1126/science.280.5369.1564
- Green, C. B., Takahashi, J. S., & Bass, J. (2008). The meter of metabolism. *Cell*, *134*(5), 728–742. doi:10.1016/j.cell.2008.08.022
- Guglielmi, V., Nowis, D., Tinelli, M., Malatesta, M., Paoli, L., Marini, M., Manganotti, P., Sadowski, R., Wilczynski, G. M., Meneghini, V., & Tomelleri, G. (2017). Bortezomib-induced muscle toxicity in multiple myeloma. *J Neuropathol Exp Neurol*, *76*(7), 620–630. doi:10.1093/jnen/nlx043
- Guo, Y., Walther, T. C., Rao, M., Stuurman, N., Goshima, G., Terayama, K., Wong, J. S., Vale, R. D., Walter, P., & Farese, R. V. (2008). Functional genomic screen reveals genes involved in lipid-droplet formation and utilization. *Nature*, *453*(7195), 657–661. doi:10.1038/nature06928
- Hanahan, D., & Weinberg, R. A. (2011). Hallmarks of cancer: The next generation. *Cell*, *144*(5), 646–674. doi:10.1016/j.cell.2011.02.013
- Heaton, N. S., Perera, R., Berger, K. L., Khadka, S., LaCount, D. J., Kuhn, R. J., & Randall, G. (2010). Dengue virus non-structural protein 3 redistributes fatty acid synthase to sites of viral replication and increases cellular fatty acid synthesis. *Proc Natl Acad Sci USA*, *107*(40), 17345–17350. doi:10.1073/pnas.1010811107
- Kiessling, S., Beaulieu-Laroche, L., Blum, I. D., Landgraf, D., Welsh, D. K., Storch, K. F., Labrecque, N., & Cermakian, N. (2017). Enhancing circadian clock function in cancer cells inhibits tumor growth. *BMC Biol*, *15*(1), 13. doi:10.1186/s12915-017-0349-7
- Kim, T. (2012). Bortezomib induces G2-M arrest in human colon cancer cells through ROS-inducible phosphorylation of ATM-CHK1. *Int J Oncol*, *41*, 76–82. doi:10.3892/ijo.2012.1448
- King, D. P., Zhao, Y., Sangoram, A. M., Wilsbacher, L. D., Tanaka, M., Antoch, M. P., Steeves, T. D., Vitaterna, M. H., Kornhauser, J. M., Lowrey, P. L., & Turek, F. W. (1997). Positional cloning of the mouse circadian clock gene. *Cell*, *89*(4), 641–653. doi:10.1016/s0092-8674(00)80245-7
- Ling, Y.-H., Liebes, L., Zou, Y., & Perez-Soler, R. (2003). Reactive oxygen species generation and mitochondrial dysfunction in the apoptotic response to Bortezomib, a novel proteasome inhibitor, in human H460 non-small cell lung cancer cells. *J Biol Chem*, *278*, 33714–33723. doi:10.1074/jbc.M302559200
- Lowrey, P. L., & Takahashi, J. S. (2004). Mammalian circadian biology: Elucidating genome-wide levels of temporal organization. *Annu Rev Genomics Hum Genet*, *5*, 407–441. doi:10.1146/annurev.genom.5.061903.175925
- Martinez-Vicente, M., Tallozy, Z., Wong, E., Tang, G., Koga, H., Kaushik, S., De Vries, R., Arias, E., Harris, S., Sulzer, D., & Cuervo, A. M. (2010). Cargo recognition failure is responsible for inefficient autophagy in Huntington’s disease. *Nature Neurosci*, *13*(5), 567–576. doi:10.1038/nn.2528
- Meijer, A. J., & Codogno, P. (2004). Regulation and role of autophagy in mammalian cells. *Int J Biochem Cell Biol*, *36*(12), 2445–2462. doi:10.1016/J.BIOCEL.2004.02.002
- Morera, L. P., Díaz, N. M., & Guido, M. E. (2016). Horizontal cells expressing melanopsin x are novel photoreceptors in the

- avian inner retina. *Proc Natl Acad Sci*, 113(46), 13215–13220. doi:10.1073/pnas.1608901113
- Portal, M. M., Ferrero, G. O., & Caputto, B. L. (2007). N-Terminal c-Fos tyrosine phosphorylation regulates c-Fos/ER association and c-Fos-dependent phospholipid synthesis activation. *Oncogene*, 26(24), 3551–3558. doi:10.1038/sj.onc.1210137
- Preitner, N., Damiola, F., Lopez-Molina, L., Zakany, J., Duboule, D., Albrecht, U., & Schibler, U. (2002). The orphan nuclear receptor REV-ERB α controls circadian transcription within the positive limb of the mammalian circadian oscillator. *Cell*, 110(2), 251–260. Retrieved from <http://www.ncbi.nlm.nih.gov/pubmed/12150932>
- Raspé, E., Duez, H., Gervois, P., Fiévet, C., Fruchart, J. C., Besnard, S., Mariani, J., Tedgui, A., & Staels, B. (2001). Transcriptional regulation of apolipoprotein C-III gene expression by the orphan nuclear receptor ROR α . *J Biol Chem*, 276(4), 2865–2871. doi:10.1074/jbc.M004982200
- Raspé, E., Duez, H., Mansén, A., Fontaine, C., Fiévet, C., Fruchart, J. C., Vennström, B., & Staels, B. (2002). Identification of Rev-erb α as a physiological repressor of apoC-III gene transcription. *J Lipid Res*, 43(12), 2172–2179. doi:10.1194/jlr.m200386-jlr200
- Sato, T. K., Panda, S., Miraglia, L. J., Reyes, T. M., Rudic, R. D., McNamara, P., Naik, K. A., FitzGerald, G. A., Kay, S. A., & Hogenesch, J. B. (2004). A functional genomics strategy reveals Rora as a component of the mammalian circadian clock. *Neuron*, 43(4), 527–537. doi:10.1016/j.neuron.2004.07.018
- Singh, R., Kaushik, S., Wang, Y., Xiang, Y., Novak, I., Komatsu, M., Tanaka, K., Cuervo, A. M., & Czaja, M. J. (2009). Autophagy regulates lipid metabolism. *Nature*, 458(7242), 1131–1135. doi:10.1038/nature07976
- Solt, L. A., Wang, Y., Banerjee, S., Hughes, T., Kojetin, D. J., Lundasen, T., Shin, Y., Liu, J., Cameron, M. D., Noel, R., & Yoo, S. H. (2012). Regulation of circadian behaviour and metabolism by synthetic REV-ERB agonists. *Nature*, 485(7396), 62–68. doi:10.1038/nature11030
- Sulli, G., Rommel, A., Wang, X., Kolar, M. J., Puca, F., Saghatelian, A., Plikus, M. V., Verma, I. M., & Panda, S. (2018). Pharmacological activation of REV-ERBs is lethal in cancer and oncogene-induced senescence. *Nature*, 553(7688), 351–355. doi:10.1038/nature25170
- Tan, S., Díaz, N. M., & Guido, M. E. (1998). The regulation of reactive oxygen species production during programmed cell death. *J Cell Biol*, 141(6), 1423–1432. doi:10.1083/jcb.141.6.1423
- Vlachostergios, P. J., Hatzidaki, E., Stathakis, N. E., Koukoulis, G. K., & Papandreou, C. N. (2013). Bortezomib downregulates MGMT expression in T98G glioblastoma cells. *Cell Mol Neurobiol*, 33(3), 313–318. doi:10.1007/s10571-013-9910-2
- Wagner, P. M., Alderete, L. G. S., Gorné, L. D., Gaveglia, V., Salvador, G., Pasquaré, S., & Guido, M. E. (2018). Proliferative glioblastoma cancer cells exhibit persisting temporal control of metabolism and display differential temporal drug susceptibility in chemotherapy. *Mol Neurobiol*, 56(2), 1276–1292. doi:10.1007/s12035-018-1152-3
- Welte, M. A., & Gould, A. P. (2017). Lipid droplet functions beyond energy storage. *Biochimica et Biophysica Acta (BBA) – Molecular and Cell Biology of Lipids*, 1862(10), 1260–1272. doi:10.1016/J.BBALIP.2017.07.006
- Woldt, E., Sebti, Y., Solt, L. A., Duhem, C., Lancel, S., Eeckhoutte, J., Hesselink, M. K., Paquet, C., Delhay, S., Shin, Y., & Kamenecka, T. M. (2013). Rev-erb- α modulates skeletal muscle oxidative capacity by regulating mitochondrial biogenesis and autophagy. *Nat Med*, 19(8), 1039–1046. doi:10.1038/nm.3213
- Yu, C., Rahmani, M., Dent, P., & Grant, S. (2004). The hierarchical relationship between MAPK signaling and ROS generation in human leukemia cells undergoing apoptosis in response to the proteasome inhibitor Bortezomib. *Exp Cell Res*, 295(2), 555–566. doi:10.1016/j.yexcr.2004.02.001
- Zhang, Y., Fang, B., Emmett, M. J., Damle, M., Sun, Z., Feng, D., Armour, S. M., Remsberg, J. R., Jager, J., Soccio, R. E., & Steger, D. J. (2015). GENE REGULATION. Discrete functions of nuclear receptor Rev-erb α couple metabolism to the clock. *Science*, 348(6242), 1488–1492. doi:10.1126/science.aab3021